

Forecasting Research

Forecasting Research Division
Technical Report No. 200

An Objective Visibility Analysis and Very-Short-Range Forecasting System

by

Bruce Wright and Nigel Thomas

October 1996

**Meteorological Office
London Road
Bracknell
Berkshire
RG12 2SZ
United Kingdom**



FR Division Technical Report No. 200

An Objective Visibility Analysis and Very-Short-Range Forecasting System

by

Bruce Wright and Nigel Thomas

October 1996

Forecasting Research Division
Meteorological Office
London Road
Bracknell
Berkshire, RG12 2SZ
England

©Crown Copyright 1996

This is an unpublished document. Permission to quote from it must be obtained from the Director of the above Meteorological Office Division.

An Objective Visibility Analysis and Very-Short-Range Forecasting System

Bruce Wright and Nigel Thomas

Meteorological Office, London Road, Bracknell, Berkshire, RG12 2SZ, UK

25th October 1996

Abstract

An objective Visibility Analysis/Forecast System has been developed as part of Nimrod, the United Kingdom Meteorological Office (UKMO) very-short-range forecasting system. The analysis blends satellite imagery and surface observations with a one hour forecast using a variational algorithm. An extrapolation forecast is produced by adding UKMO Mesoscale Model trends to the analysis values. This is merged with persistence (the analysis) and Model values, to produce the final forecast. Results from 8 case studies are presented, showing the potential of the system, which demonstrates significant improvements on the Model predictions (the currently available objective forecast method).

1 Introduction

In 1992 a five year project was initiated within the United Kingdom Meteorological Office (UKMO) to produce a computer-based system which would give human forecasters the best guidance possible when issuing forecasts in the range 0–6 hours ahead for the United Kingdom and surrounding waters. This project was called Nimrod (Golding 1995, Golding 1996*a*). It was to produce analyses and forecast guidance for a number of meteorological parameters such as precipitation (Ryall 1994, Golding 1996*b*), cloud (Pamment 1994), including the provision of cloud data for assimilation by the Mesoscale Model (Macpherson, Wright, Hand & Maycock 1996), and visibility. The system was to make use of as many different sources of data as necessary in order to give the best analyses possible, and then use these analyses and other data to produce forecasts of the parameters concerned. The forecasts were designed to slowly merge with the UKMO Mesoscale Model forecast so that continuity would be maintained beyond the six hour forecast time when the Model became the main source of guidance. This paper describes the analysis and forecasting methods used for the visibility element of the project and reports the results of a number of case studies.

2 Scope

The UKMO Mesoscale Model is a version of the Unified Model (Cullen 1990, Lorenc, Bell & Macpherson 1991), which is used for all UKMO NWP and climate research applications. It has a grid-spacing of approximately 17 km, covering the British Isles, the North Sea and parts of the near-continent, and provides forecasts of visibility four times a day out to between 18 and 30 hours, which are available within 4 hours of the data time. It uses a reasonably sophisticated cloud scheme to partition the conserved temperature and moisture variables into temperature, humidity and liquid water (Smith 1990). From these variables and a three-dimensional aerosol field, visibility is diagnosed using a scheme developed by Clark (personal communication), which is described in detail in section 4.1.

Nimrod will provide forecasts of visibility in half-hourly steps out to 6 hours, which will be available within 40 minutes of data time. This is performed on a 5 km National Grid, covering an area similar to the domain of the Mesoscale Model (figure 1). Although the required product is a continuous visibility variable, particular emphasis is placed on the prediction of fog. No attempt has been made to properly treat hill fog, which, being cloud, should be handled by the Cloud Analysis/Forecast component of Nimrod. However, it is impossible to exclude hill fog from the visibility component.

3 Visibility and Fog

Visibility is determined primarily by the moisture and aerosols present in the atmosphere. In unsaturated air, the visibility is determined by the relative humidity and the aerosols. In saturated air (fog), the liquid water mixing ratio and droplet spectrum become important. However, in devising a scheme for both the analysis and prediction of visibility, it is useful to consider the important processes involved in the physics of fog. There is a large body of literature covering the subject (e.g. Roach, Brown, Caughey, Garland & Readings (1976) and Brown & Roach (1976)). The following summary is based on chapter 2 of an M.Sc.

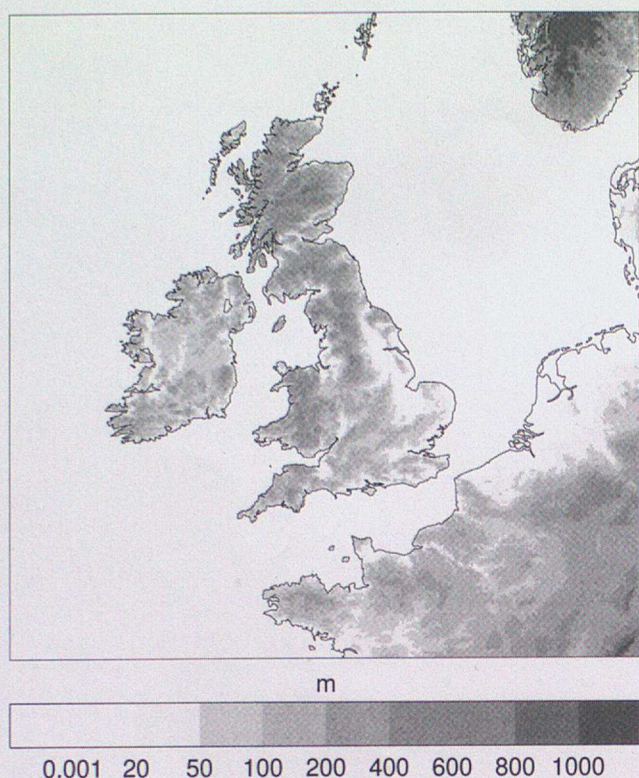


Figure 1: The Nimrod domain and orography.

dissertation by Thomas (1995).

3.1 Fog formation

There are three main mechanisms for the formation of fog. These are listed below, with the type of fogs which tend to be associated with the particular mechanism given in parentheses:

- Cooling the air to its dew point (radiation fog and advection fog)
- Addition of water vapour to the air (frontal fog)
- Vertical mixing of moist air parcels of different temperatures (advection fog and thickening of most fogs)

One way of characterising all of these effects is to consider variations in the temperature, T , and the dew point temperature, T_d , of the air.

The formation of radiation fog has been quite widely studied (Roach et al. 1976, Fitzjarrald & Lala 1989). As with the formation of all types of fog, it is relative humidity which is crucial, but its evolution is primarily governed by that of the temperature in the case of radiation fog. The ground cools by emitting long-wave radiation to space. The near-surface air cools by radiating to the ground, until the dew point temperature is reached and water vapour condenses to form fog droplets. This is complicated by the production

of dew beforehand, which has the effect of drying the air and lowering the dew point temperature. The formation of radiation fog is determined by the balance between the increase in the relative humidity of the air through radiative cooling, and the drying of the air through dew deposition. The processes involved are affected by other variables, such as wind speed and cloud cover. The formation of radiation fog is very localised, making the prediction of temperature at a high resolution very important (and to some extent dew point, although typically this is a smoother field).

In both frontal fog and advection fog, the air often experiences a moistening as well as cooling. In frontal fog, this is because of the evaporation of precipitation. In advection fog, this is usually because of mixing the main air mass with a cooler near-surface layer (e.g. warm air moving over a cool sea surface or snow-covered land). Probably the most common example of an advection fog is sea fog (e.g. the Haar of the northern and eastern coasts of Scotland (Findlater, Roach & McHugh 1989)). However, although both temperature and dew point variations are important in these processes, they tend to occur over a fairly large area, making the prediction of high resolution temperatures and dew points less important than in the case of radiation fog. Consequently, the processes involved are better represented in Mesoscale Model predictions than those for radiation fog.

3.2 Fog Evolution

Once fog water is present, the fog can be characterised by its temperature (or its dew point, which is identical), the cloud water mixing ratio, q_L , and the droplet size spectrum.

The presence of fog droplets completely changes the radiative properties of the surface layer, with the ground and fog droplets simultaneously radiating. When a fog has become optically thick (usually about 20–50 m deep for a radiation fog), the ground is effectively shielded from radiative loss, and all the cooling is by radiation from the fog droplets. Persistent fogs which start as advection fogs usually become radiation fogs as they become optically thick and cooling by radiation from fog droplets takes over as the dominant sustaining mechanism. If this cooling continues, the fog will deepen and knowledge of the temperature and cloud water profiles through the fog is required to fully describe it. Alternatively, if assumptions are made about the shape of these profiles a single additional variable representing the fog depth or the vertically integrated fog water content will suffice.

This mode of evolution is not generally true for frontal fogs, for which the incoming long-wave radiation from cloud tends to balance the radiation from the fog droplets. The main process of modification

of frontal fog, once it has formed, is advection. This, once again, is a large scale effect, and so it should not be too difficult to represent.

3.3 Fog Clearance

The main mechanism for fog clearance locally is evaporation, although the fog may also be advected away. Evaporation is caused by either a warming of the air, or a drying of the air. The warming is because of either solar radiation after sunrise, or long-wave radiation from an over-lying cloud sheet. In general, there is also a heat flux from the soil, but this is smaller and, although it will contribute, not usually responsible for a clearance of fog. Drying of the air is caused by the turbulent mixing of dry air from above or at the edge into the fog. This happens when the gradient wind increases. All of these processes are somewhat complicated by the lifting of the fog to low stratus, which often occurs when the fog is well-mixed and the bottom becomes unsaturated first; this does require the air above the fog to be fairly moist.

The warming effects of incoming radiation are energy inputs which act on a large scale (in general), as does an increase in gradient wind speed. However, some knowledge or guess of the fog depth or integrated water content is required in order to predict the time taken for the clearance. Advection of the fog may also be a large-scale effect, although local flows (often topographically related) may be important.

4 The Approach

4.1 Prognostic Variables

As discussed in section 3, fog formation can be characterised by the temperature, T , and dew point temperature, T_d , and fog evolution and clearance by the temperature, T , cloud water mixing ratio, q_L , and fog depth, d . One way of simplifying this characterisation is to use variables which are conserved through condensation, such as liquid water temperature, T_L , and total water mixing ratio, q_t , which are defined by the equations:

$$T_L = T - \frac{Lq_L}{C_p} \quad (1)$$

$$q_t = q + q_L \quad (2)$$

where q is the specific humidity mixing ratio, L is the latent heat of condensation and C_p is the specific heat capacity at constant pressure. Strictly speaking, equations 1 and 2 should include terms representing the contribution from the ice phase, but as ice fog is very

rarely observed in the UK, the ice phase has been neglected throughout. T_L and q_t provide a full description of the grid-box mean temperature and moisture environment. In unsaturated air, T_L is simply the temperature and q_t the humidity mixing ratio of the air. When condensation occurs, the situation is slightly more complicated, as both T_L and q_t depend on q_L , but it is still possible to recover T , q and q_L , given certain assumptions.

It is reasonable to assume that within a grid-square, with a mean state characterised by T , q and q_L , a range of states exist locally. This allows for temperature and moisture variations at a scale below that explicitly represented, and means that it is possible for cloud water to be present even when the mean state of the grid-box is unsaturated. The cloud scheme used within the Mesoscale Model (Smith 1990) assumes a triangular distribution of states, characterised by a critical relative humidity, RH_{crit} (91.64% at the surface); RH_{crit} represents the mean grid-box relative humidity above which cloud water is present. This scheme has been adopted within Nimrod to recover the temperature and moisture variables, but with a larger value of RH_{crit} (94%) to take account of the smaller grid-spacing. In the Mesoscale Model, visibility is diagnosed from T , q and q_L and the Model aerosol variable, m , using a scheme developed by Clark (personal communication), which is based on that described by Ballard, Wright & Golding (1992), and is outlined below; this has also been adopted for use within Nimrod.

Both relative humidity and liquid water mixing ratio can be related to a mean fog droplet radius, r . For unsaturated air ($q_L = 0.0$), the relative humidity is related to the mean droplet radius, r , by the equilibrium equation (Pruppacher & Klett 1978):

$$RH = \exp \left(\frac{A_o}{r} - \frac{B_o}{\left(\frac{r}{r_d}\right)^3 - 1} \right) \quad (3)$$

where r_d is the mean volume radius of the dry aerosol, A_o is a constant ($1.2 \times 10^{-9} m$) and B_o is the Activation Parameter (0.5). The first term is neglected as small. Further, it is assumed that r_d varies as a power of the aerosol mass concentration, as follows:

$$r_d = r_o \left(\frac{m}{m_o} \right)^p \quad (4)$$

where r_o is the radius of a standard aerosol particle ($0.16 \times 10^{-6} m$), p is the power used to represent the variation in aerosol particle size with mass-loading ($\frac{1}{6}$), and m_o , standard mass mixing ratio of the aerosol ($kg.kg^{-1}$), is given by:

$$m_o = \frac{4}{3} \pi r_o^3 \left(\frac{\rho}{\rho_a} \right) N_o \quad (5)$$

where N_o is the standard number density of the aerosol ($5.0 \times 10^8 \text{ m}^{-3}$), ρ is the density of the aerosol (1700 kg.m^{-3}) and ρ_a is the density of air. This yields the following relation between the mean droplet radius and the relative humidity:

$$r = r_o \left(1 - \frac{B_o}{\ln(\text{RH})} \right)^{\frac{1}{3}} \left(\frac{m}{m_o} \right)^p \quad (6)$$

For saturated air ($q_L > 0.0$), assuming all aerosol particles are activated (the error will be small if the majority are activated), the equation is:

$$r = \left(\left(\frac{m}{m_o} \right)^{3p} r_o^3 + \frac{q_L}{\frac{4}{3}\pi\rho_w N} \right)^{\frac{1}{3}} \quad (7)$$

where ρ_w is the density of water (1000 kg.m^{-3}) and the number density of the aerosol, N , (m^{-3}) is given by:

$$N = N_o \left(\frac{m}{m_o} \right)^{(1-3p)} \quad (8)$$

The aerosol mass mixing ratio, m (kg.kg^{-1}), is taken from the Mesoscale Model, where it is modelled as a three-dimensional variable, using climatological sources and boundary conditions, tracer advection, boundary layer diffusion and a simple treatment of dry and wet deposition. However, it should not be considered as a 'true' representation of all airborne particles, but rather a useful variable for the diagnosis of visibility.

From the fog droplet radius, the visibility, Vis , is calculated using the expression (Koschmeider 1924):

$$\text{Vis} = \frac{\ln \epsilon}{N r^2 \beta_o} \quad (9)$$

where ϵ is the liminal contrast (0.02) and the scattering coefficient of normalisation, β_o , is given by:

$$\beta_o = \pi Q \eta \quad (10)$$

where Q and η represent the scattering efficiency and the effect of the aerosol particle size distribution respectively, with $Q \times \eta$ taking the value 1.5.

Thus, the scheme adopted here for the analysis and prediction of visibility, uses liquid water temperature (T_L) and total water mixing ratio (q_t) as prognostic variables, only diagnosing visibility at the final stage. The fact that neither T_L nor q_t are observed variables complicates the use of observations within the analysis slightly, but allows the system to also predict temperature and dew point (not considered in this paper).

5 The Analysis

5.1 Scheme

Analyses are made using a variational approach, blending data from satellite and surface observations, and from the forecast step of the system. The 1 hour forecast forms the first-guess. Each analysis is of T_L and q_t and is carried out using the '2DVAR' analysis scheme (Shurlock & Lorenc 1994). This utilizes a descent algorithm (*E04DGF—NAG Fortran Library Routine Document* n.d.) to minimize a penalty function, which measures the fit of the analysis to the data in terms of T_L and q_t . In order to ensure a similar weighting between the two analysis variables, q_t is scaled by 2500 (and its error variance by 2500^2) to make it of the same order as T_L .

In the following, w is the general analysis variable for which a solution is sought; it contains both T_L and q_t . The penalty function, J , consists of a number of quadratic terms (based on the assumption of a Gaussian error distribution), one for each data source, which measure the distance of the analysis from the data ($w_{\text{data}} - w$). The penalty function term for a particular data type, J_{data} , involves the error covariance matrix, O_{data} , and takes the form:

$$J_{\text{data}} = \frac{1}{2} (w_{\text{data}} - w)^T O_{\text{data}}^{-1} (w_{\text{data}} - w) \quad (11)$$

To make the problem more easily soluble, the error covariance matrix can be replaced by the error variance, E_{data} , with the error correlations being approximated by the action of a filter; the inverse of error correlation is represented by an inverse filter (or de-smoother), T_{data} . Thus, the error covariance matrix can be expressed in the form:

$$O_{\text{data}}^{-1} = T_{\text{data}}^T T_{\text{data}} E_{\text{data}}^{-1} \quad (12)$$

A two-pass recursive filter is used here to represent the error correlations, hence T is the inverse of a 1-pass recursive filter. The penalty function term takes the form:

$$J_{\text{data}} = \frac{1}{2} (T_{\text{data}}(w_{\text{data}} - w))^T E_{\text{data}}^{-1} (T_{\text{data}}(w_{\text{data}} - w)) \quad (13)$$

To improve the convergence of the solution within the NAG routine which carries out the minimisation, the penalty function can be re-written in terms of a well-conditioned variable, v . This variable takes into account the correlations of the data sources, and is computed by applying the de-smoother, T , to the 'analysis increment' (the difference between the analysis value,

w, and the first-guess value, w_{fg}), as follows:

$$v = T(w - w_{fg}) \quad (14)$$

Effectively it is a 'roughened' version of the analysis increment. The penalty function term now becomes:

$$J_{data} = \frac{1}{2} [T_{data} (w_{data} - (w_{fg} + T^{-1}v))]^T E_{data}^{-1} [T_{data} (w_{data} - (w_{fg} + T^{-1}v))] \quad (15)$$

For observations which are considered uncorrelated, the error covariance becomes simply an error variance, and T_{data} is absent. Further operators and their transposes may be necessary to map the analysis variable on to the observed variable in other cases (e.g. an interpolation operator for the surface observations).

The three components combined within the analysis scheme, i.e. the forecast, surface observations and a satellite-derived fog-mask, are discussed in the following sections.

5.2 Forecast Data

The visibility forecast (section 6) provides predictions of T_L and q_t , which should be the best first-guess for the analysis. If the 1 hour forecast is unavailable, the Mesoscale Model forecast values are used instead. Mesoscale Model screen-level pressure, aerosol mass mixing ratio and surface temperature are used, in either situation, the former two parameters in the diagnosis of visibility, the latter in the processing of the satellite data.

The penalty function term for the forecast, J_f , takes the form:

$$J_f = \frac{1}{2} [T_f (w_f - (w_{fg} + T^{-1}v))]^T E_f [T_f (w_f - (w_{fg} + T^{-1}v))] \quad (16)$$

where w_{fg} is the first-guess value of the analysis variable, w_f is the forecast value of the analysis variable, E_f is the forecast error variance, T_f is a de-smoother representing the effect of correlated forecast errors, and T and v have been defined earlier. As stated above, w_{fg} is actually set equal to w_f , so the penalty function simplifies slightly.

The quality of the forecast predictions can be very variable, and so they are assessed against surface observations, the most reliable source of information. The Root Mean Square Factor Error (RMSFE) for visibility is used to provide a value for the error variance used for the forecast. The visibility RMSFE is

given by:

$$\text{RMSFE} = \exp \sqrt{\frac{\sum_{i=1}^n \left(\ln \left(\frac{F_i}{O_i} \right) \right)^2}{n}} \quad (17)$$

where O_i is the observed value i , F_i is the value of the field (Model or forecast) interpolated to the observation point, and n is the number of observations. Only points where either the interpolated field or the observed visibility is 5 km or less are used, and values greater than 10 km are limited to 10 km. All eligible observations within the Nimrod domain are used. An error variance for T_L based on the RMSFE is then set using the following empirical relationship:

$$E_{\text{RMSFE}} = A(\text{RMSFE} - 1.0) + B \quad (18)$$

where A and B are constants: A equals 1.0 K^2 and B equals 1.0 K^2 . To allow for the small number of eligible observations which are available on occasions, the error variance is relaxed back to a default value, E_d (3.0 K^2), if there are less than n_{\min} (20) observations, using the equation:

$$E_{TL} = \alpha E_{\text{RMSFE}} + (1.0 - \alpha) E_d \quad (19)$$

where the weighting factor is given by:

$$\alpha = \frac{n}{n_{\min}} \quad (20)$$

where n is the number of eligible observations.

A basic filter scale, λ_{\max} , of 3 grid-lengths (15 km) is used to represent error correlations, although this is relaxed to 1 grid-length (5 km) over steep orography, to reduce problems caused by the inappropriate spreading of data (e.g. 'valley fog' onto the mountain-tops). A mean height difference, Δh , is calculated between the current pixel and the 8 surrounding pixels. This is used to determine the filter scale for the pixel (in grid-lengths), λ , using the following equation:

$$\lambda = \text{MAX} \left(1, \lambda_{\max} - \frac{\Delta h}{h_{\max}} (\lambda_{\max} - 1) \right) \quad (21)$$

where h_{\max} is a constant set to 200 m. Figure 2 shows the filter scales generated for the Model; these filter scales are also used to condition the analysis variables.

5.3 Satellite Data

Various approaches have been explored in attempting to recover fog from both geostationary and polar orbiter satellite imagery (e.g. Ellrod (1995), Dybbroe (1993)). A pragmatic approach is adopted here to ob-

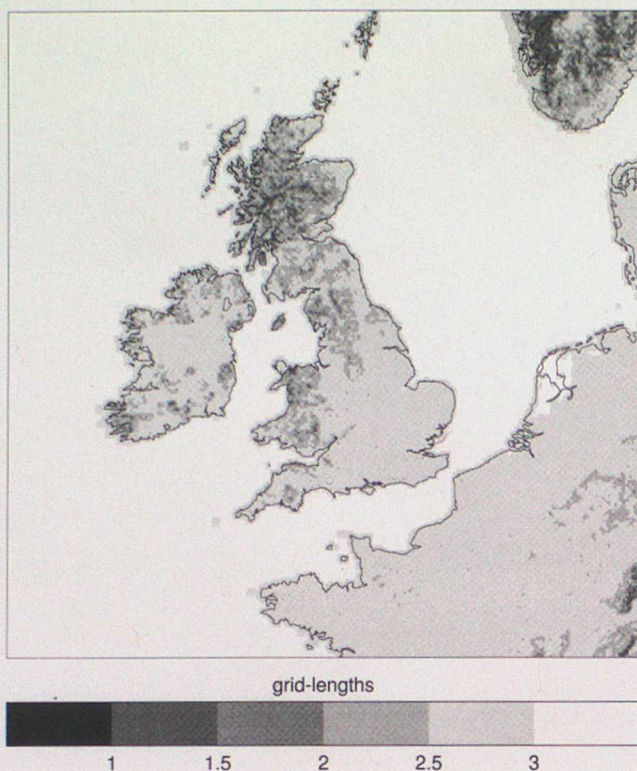


Figure 2: The filter scale used to represent the forecast correlation scales within the analysis.

tain information from both Meteosat and AVHRR imagery. This includes using the UKMO 'fog' product, which is the difference in brightness temperature between AVHRR channels 3 and 4 (centred about $3 \mu\text{m}$ and $11 \mu\text{m}$ respectively), and distinguishes fog and low cloud from other surfaces (Eyre, Brownscombe & Allam 1984). An innovative use of surface observations is made to 'calibrate' the data.

The satellite data are taken from one of two sources depending on availability. In the day, Meteosat visible and infrared imagery are used. At night, the AVHRR fog product and infrared image are used, when available (currently twice per night, usually about 02 UTC and 04 UTC). The most reliable source of information on the presence of fog is surface observations. These are used to 'calibrate' the satellite data. The classification of fog/clear/unknown is carried out in three stages:

1. the diagnosis of medium or high cloud
2. the diagnosis of fog/cloud and clear areas
3. the diagnosis of fog

The diagnosis of medium or high cloud is a very coarse 'flagging' of those pixels for which no useful information on the presence or absence of fog exists. The difference between the satellite infrared temperature and the Model surface temperature is compared with a fixed threshold (which could be different for

land and sea areas). If the threshold is exceeded, the pixel is flagged 'cloudy'. A threshold value of 15°C is used at present.

The diagnosis of fog/cloud and clear pixels is a simple comparison of the visible or fog image value with a threshold value. This involves a somewhat different treatment for the Meteosat and AVHRR imagery. For Meteosat visible imagery a threshold value of 100 (in normalised raw counts) is used; values below this are flagged clear, values above are flagged cloudy. For the AVHRR imagery, a threshold value of 15 (in non-meaningful units) is used, but values below this are flagged as missing data, rather than clear; values above the threshold are flagged cloudy. This difference is because negative values in the AVHRR fog imagery indicate high cloud, and so setting to 'clear' can lead to errors.

Finally, a classification into the categories fog, clear and unknown is carried out. The 'satellite fog' is set to clear, where the 'fog/cloud mask' is clear. Pixels flagged either as missing data in the fog/cloud mask or as cloudy in the 'medium/high cloud mask' are assumed to have no useful information on the presence of fog, and so are set to missing data in the satellite fog field. The flagging of pixels as cloudy in the fog/cloud mask indicates the presence of either fog or low cloud, and surface observations are used to predict which. Observations of visibility, which are co-located with this 'potential fog' or have visibilities of 1000 m or less are used (the latter is to allow for patchy fog which is not perfectly co-located with the 'satellite fog'). Potentially foggy pixels are assigned the visibility of the nearest such report. However, this 'calibration' is limited to a 20 pixel (100 km) radius, and only land points (to stop land visibilities being spread 'out to sea'). Any pixels which remain undetermined are set to missing data. Figure 3 shows the various stages of the satellite processing, with surface observations for comparison for 12 UTC on 23rd December, 1994, a case which uses Meteosat data.

The penalty function for the satellite data, J_s , which can be written in terms of implied differences from the analysis values of T_L and q_t : ΔT_L and Δq_t respectively (these will be discussed later), is given by the equation:

$$J_s = \frac{1}{2} [T_s (\Delta T_L)]^T E_s [T_s (\Delta T_L)] + \frac{1}{2} [T_s (q_{t_{scaling}} \Delta q_t)]^T \frac{E_s}{q_{t_{scaling}}^2} [T_s (q_{t_{scaling}} \Delta q_t)] \quad (22)$$

where T_s is the square root of the inverse filter (de-smoother) used to represent the error correlations, and E_s is the error variance assigned to the satellite data (in K^2). Where the satellite data incur a penalty, T_L and q_t are assigned error variances of 1.0 K^2 and $1.6 \times 10^{-7} \text{ kg}^2 \cdot \text{kg}^{-2}$ respectively, and a filter scale of 1 grid-

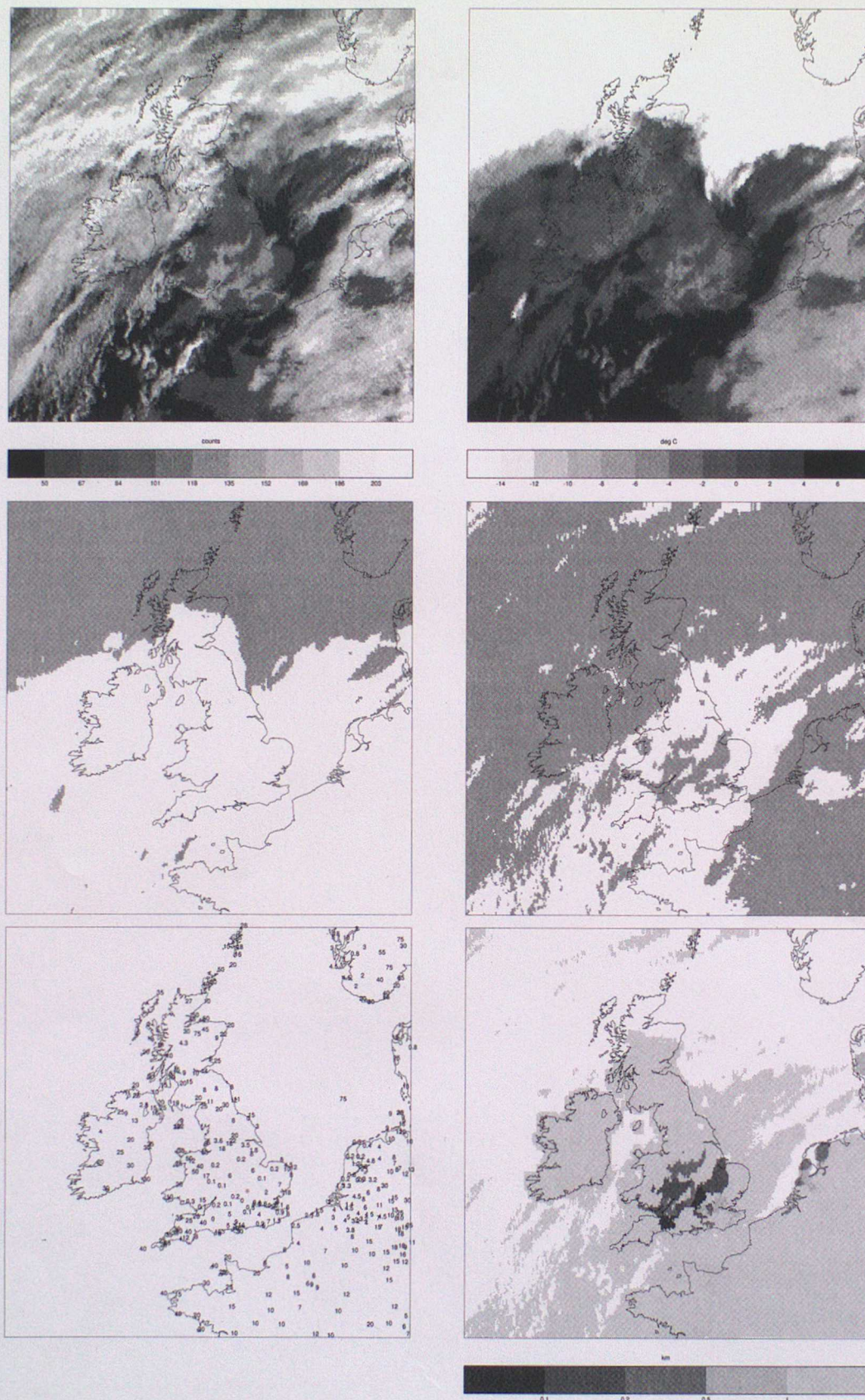


Figure 3: Satellite imagery processing for 12 UTC 23rd December, 1994. TOP LEFT: Meteosat visible image, TOP RIGHT: Meteosat infrared image, MIDDLE LEFT: satellite-derived medium/high cloud mask (grey = cloud, white = unknown), MIDDLE RIGHT: satellite-derived fog/low cloud and clear (grey = fog/cloud, white = clear). BOTTOM LEFT: Surface SYNOP reports of visibility (km) for comparison purposes, BOTTOM RIGHT: satellite-derived visibility product: (visibilities greater than 1000 m and clear areas are shown in light grey (see legend); white indicates missing data)

length (5 km) is used to represent error correlations.

Pixels which have not been assigned a visibility, or have been assigned a visibility greater than 1000 m have values of zero for ΔT_L and Δq_t (i.e. incur no penalty). Those pixels diagnosed clear are weighted towards non-saturation. This is carried out by defining limits for T_L and q_t (equations 23 and 24).

$$T_L \geq T_{L_{limit}} = T_{sat} \left(\frac{q_t}{RH_{crit}} \right) \quad (23)$$

$$q_t \leq q_{t_{limit}} = RH_{crit} q_{sat}(T_L) \quad (24)$$

where T_{sat} is the temperature at which a parcel is saturated, as a function of humidity mixing ratio, and q_{sat} is the saturated humidity mixing ratio, as a function of temperature. If the analysed T_L is greater than $T_{L_{limit}}$ (the analysis is also unsaturated), then, once again, ΔT_L and Δq_t are set to zero, and no penalty is incurred, otherwise analysis differences are calculated using equations 25 and 26

$$\Delta T_L = \frac{1}{2} (T_{L_{limit}} - T_L) \quad (25)$$

$$\Delta q_t = \frac{1}{2} (q_{t_{limit}} - q_t) \quad (26)$$

Pixels assigned visibilities below 1000 m are weighted towards mean grid-scale saturation. Once again, this is carried out by defining limits for T_L and q_t (equations 27 and 28).

$$T_L \leq T_{L_{limit}} = T_{sat}(q_t) \quad (27)$$

$$q_t \geq q_{t_{limit}} = q_{sat}(T_L) \quad (28)$$

This is equivalent to about half cloud cover. Weighting towards 'full cloud cover' was found to force the visibilities to be too low, whereas weighting towards saturation did not force the visibilities to be low enough. If the analysed T_L is less than $T_{L_{limit}}$ (the analysis is also saturated), then ΔT_L and Δq_t are set to zero, otherwise equations 25 and 26 are used to calculate the analysis differences.

5.4 Surface Observations

Surface observations of visibility, temperature, dew point and pressure from SYNOP and SHIP reports are used within the analysis. Visibilities are adjusted to the mid-value of the range they represent (e.g. a report of 01 is interpreted as 150 m), before being used. If no visibility is reported or the observed visibility is

greater than 10 km, then temperature and dewpoint are used to derive T_L and q_t . In this case, a 'critical temperature', at which condensation would start occurring locally, is calculated from the temperature and RH_{crit} . If the temperature is above this, then T_L is set to the temperature and q_t to the humidity mixing ratio. Otherwise, T_L and q_t are set to minus these values; this acts as a flagging procedure, so that the absolute values are used as limits (in the same way as the satellite data). If a visibility of 10 km or below is reported, then re-arranged forms of equations 6, 7 and 9 are used to recover a relative humidity and a liquid water mixing ratio from the visibility and temperature, as follows. Equation 29 gives a mean fog droplet radius, r .

$$r = \left(\frac{\ln \epsilon}{Vis N \beta_o} \right)^{\frac{1}{2}} \quad (29)$$

This can be used to produce values for either relative humidity, RH (equation 30), or liquid water mixing ratio, q_L (equation 31),

$$RH = \exp \left(\frac{B_o}{1 - \left(\frac{r}{r_o} \right)^3 \left(\frac{m_o}{m} \right)^{3p}} \right) \quad (30)$$

$$q_L = \frac{4}{3} \pi \rho_w N \left(r^3 - \left(\frac{m}{m_o} \right)^{3p} r_o^3 \right) \quad (31)$$

where the variables are those defined in section 4.1. If the derived relative humidity is below RH_{crit} then T_L and q_t are set using the temperature and this humidity. Otherwise, the temperature and the derived liquid water mixing ratio are used. This approach means that at 10 km and below the T_L and q_t values going into the analysis from the observation are closely tied to the observed visibility. At higher visibilities, this is unsafe, and so they are based on the observed temperature and dew point. This also ensures that T_L and q_t values are still available when no visibility is provided (i.e. maximum use of surface observations is made). The Mesoscale Model aerosol mixing ratio is interpolated to observation points and used within this process.

The penalty function for the surface observations takes the form:

$$J_o = \frac{1}{2} [y_o - K(w_{fg} + T^{-1}v)]^T E_o [y_o - K(w_{fg} + T^{-1}v)] \quad (32)$$

where w_{fg} is the first-guess value of the analysis variable, y_o is the value of the analysis variable derived from surface observations at the observing points, E_o is the surface observation error variance, K is the in-

	Persistence	Mesoscale Model	Extrapolation Forecast
A	1.0 K ²	1.0 K ²	1.0 K ²
B	1.0 K ²	0.0 K ²	1.0 K ²
E_d	3.8 K ²	5.7 K ²	3.8 K ²
ΔE_{TL}	1.0 K ²	0.0 K ²	0.4 K ²

Table 1: A, B and E_d are the parameters used in the calculation of the error variances which form the weights for the merging of the three components of the forecast: Persistence, Model and extrapolation forecast. ΔE_{TL} is the increase applied to those error variances per hour into the forecast.

terpolation operator which transforms from the Nimrod grid to the observation points, and the other variables have their usual meanings. The surface observations are considered to be the most accurate data, by far, and thus are assigned a high weight; T_L and q_t are given error variances of 0.25 K² and $4.0 \times 10^{-8} \text{ kg}^2 \cdot \text{kg}^{-2}$ respectively.

6 The Forecast

Forecasts are generated using the prognostic variables T_L and q_t . They are formed by merging three components with varying weights, which depend on their relative quality. The three components are the analysis, which represents persistence, the most recent Mesoscale Model prediction and an extrapolation forecast (described below). The weight assigned to each component is assessed using the performance of a '1 hour forecast' from the previous hour (in practice, the analysis for the previous hour, the Model forecast valid at the current hour and a 1 hour extrapolation forecast from the previous hour). Comparison is made with all the surface observations of visibility within the Nimrod domain. The RMSFE for visibility is used to set an error variance for each of the components using equations 17 to 20 as described in section 5.2; the values of the various parameters are given in table 1. The constant B is an adjustment to the error variance and is set to 0.0 K² for the Model, but 1.0 K² for persistence and the extrapolation forecast. This allows for the correlations which exist between the persistence and extrapolation forecasts at the observation points, because of the use of the previous hour's observations; this will tend to suggest that these fields have a higher quality than is the case. Fixed trends are applied to these 'T+1 error variances' (ΔE_{TL} per hour) over the forecast period in order to simulate the error growth in each data source (see table 1); the 0.0 K² value for the Model reflects the fact that the Model quality is approximately constant over the 6 hour time scale considered here, whereas the quality of the other components falls off with time. The three components are merged to give the final forecast value for the liquid

water temperature, T_L , using equation 33.

$$T_L = \frac{\left(\frac{T_{L_{per}}}{E_{per}}\right) + \left(\frac{T_{L_{model}}}{E_{model}}\right) + \left(\frac{T_{L_{ext}}}{E_{ext}}\right)}{\left(\frac{1}{E_{per}}\right) + \left(\frac{1}{E_{model}}\right) + \left(\frac{1}{E_{ext}}\right)} \quad (33)$$

where the $T_{L_{per}}$, $T_{L_{model}}$ and $T_{L_{ext}}$ are the values of liquid water temperature produced by persistence, the Model and the extrapolation forecast respectively, and E_{per} , E_{model} and E_{ext} are their corresponding error variance values. The merging of q_t is carried out in the same way, but the error variance values are divided by 2500². Visibility is derived from T_L and q_t using the Model aerosol following the method described in section 4.1.

The extrapolation forecast is produced under the assumption that the Model displays the correct trends in the prognostic variables, T_L and q_t , although not necessarily the true values of the variables. The analysis gives a more accurate representation of T_L and q_t , but, by definition, is only available at analysis time. Thus, adding the Analysis minus Model differences in T_L and q_t (calculated at T+0) to the Model predictions at later times can be used to refine the Model forecast. More sophisticated methods of generating 'corrected' forecast values were explored, but found to give little benefit. These 'corrected' Model predictions form the extrapolation forecast, which is merged with persistence and the Model, as described above.

7 Case Studies

The Nimrod Visibility Analysis/Forecast System (VAFS) was tested on 8 distinct case study periods, giving 92 hours of analyses and 14 6-hour forecasts to be verified. Table 2 provides a summary of the cases, which were chosen to cover a range of different meteorological conditions relevant to fog formation, development and clearance. It also indicates the times for which satellite data were available for use within the analysis (a rather small number in the winter cases). The analysis/forecast cycle is started an hour before start verification time to provide a merged 1 hour forecast as input to the first verified analysis and to allow the weights for the merging to be calculated on a skill-basis. A Model prediction replaces the merged forecast to start the procedure. A one hour 'spin-up' period is rather short, and 'contamination' from poor Model predictions is evident in some of the cases.

7.1 Objective Statistics

A number of objective statistics are used in the verification; these are defined here. For assessing the prediction of fog at 1000 m and 200 m thresholds, the Hit Rate (HR) (also known as Probability of Detection),

Case Date	Analysis Times	Forecast Data Times	Satellite Data Available	Case Description
23/12/94	00–18	00, 06, 12	12, 13	Widespread, persistent freezing fog with an orographic dependence. Handled poorly by the Model
24/7/95	01–07 17–23	01 17	02, 03, 07 17, 18	No fog (null) case — sunrise and sunset
13–14/10/95	18–12	18, 00, 06	02, 03, 10, 11, 12	Widespread radiation fog
15/10/95	00–06	00	02, 04	Poor visibilities in warm sector being cleared by cold front approaching from the west
9/11/95	02–08	02	02, 04	Poor visibilities in warm sector to south of near stationary front lying across the country
13/11/95	04–10	04	10	Fog in warm sector southeasterly flow ahead of front
28/12/95	03–21	03, 09, 15	04, 12	Regions of persistent freezing fog

Table 2: Summary of case studies, showing date, the period for which analyses were generated, the times at which 6-hour forecasts were initiated, the times for which either Meteosat or AVHRR satellite data were available, and a brief case description.

False Alarm Rate (FAR) and the Critical Success Index (CSI) scores are used:

$$HR = \frac{\text{Correctly predicted 'foggy'}}{\text{Observed 'foggy'}} \quad (34)$$

$$FAR = \frac{\text{Incorrectly predicted 'foggy'}}{\text{Predicted 'foggy'}} \quad (35)$$

$$CSI = \frac{\text{Correctly predicted 'foggy'}}{\text{Observed or predicted 'foggy'}} \quad (36)$$

To assess the prediction of the continuous visibility field, up to 10 km, two useful statistics are the Mean Factor Error (MFE) and Root Mean Square Factor Error (RMSFE):

$$MFE = \exp \left(\frac{\sum_{i=1}^n \ln \left(\frac{\text{Field}_i}{\text{Truth}_i} \right)}{n} \right) \quad (37)$$

$$RMSFE = \exp \sqrt{\frac{\sum_{i=1}^n \left(\ln \left(\frac{\text{Field}_i}{\text{Truth}_i} \right) \right)^2}{n}} \quad (38)$$

In the verification these are only calculated for points where either the field being verified or the 'true value' is 5 km or below, and values greater than 10 km are limited to 10 km. This is to prevent the scores being biased towards errors in high visibilities.

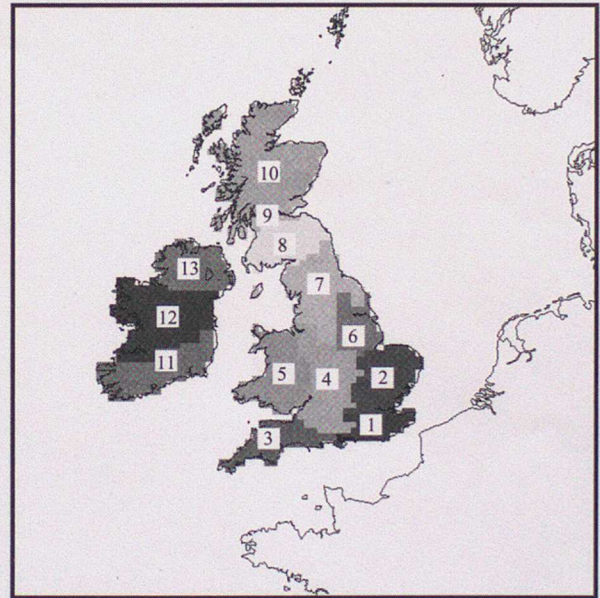


Figure 4: The 13 different regions used for area-based verification.

7.2 Analysis Verification Results

The visibility analysis was assessed against British Isles SYNOP reports, using an area-based scheme in which the land is split into 13 geographical regions (figure 4). Only the predominately low-land areas (1,2,3,4,6,9,12,13) were objectively assessed, but all areas were assessed subjectively, and all available British Isles observations were used to generate point-based statistics. For the objective assessment, a region was classified as 'foggy' if at least 30% of the pixels (observations) in that region had visibilities below the required threshold, and was classified clear otherwise (visibility observations were adjusted to represent the middle of their valid range before being used). From

Source	Obs	MeanF	RMSF
Nimrod analysis	3468	1.00	2.24
Mesoscale Model	3908	2.72	5.7

Table 5: Analysis point-based Mean Factor Error and Root Mean Square Factor Error for all cases. 'Obs' indicates the number observations used in the calculation of the statistics.

this, Hit Rate (HR), False Alarm Rate (FAR) and Critical Success Index (CSI) were calculated. Thresholds of 1 km and 200 m were used.

The results are presented in table 3, for the Nimrod analysis and the Model prediction which would be available operationally (T+4 to T+10 hours). At the 1000 m threshold, the analysis scores are significantly better than the Mesoscale Model, as would be expected. However, at the 200 m threshold, the HR, FAR and CSI are very similar to the Model scores, and very poor. The immediate implication is that the analysis is seriously under-detecting the thick fog. However, similar statistics for the point-based comparison (table 4) show that the 200 m fog is being fitted as well as the 1000 m fog at observation locations. Therefore, the discrepancy is in the perceived areal extent of the fog. Thick fog tends to be more patchy, and the siting of the observing stations may mean that the 'observed' areal extent of the fog implied by the assessment procedure is too great. 20 of the 35 foggy regions arise from a single case (23/12/94) in which the distribution of fog was highly influenced by orography (see section 7.4). These facts suggest that the handling of the 200 m fog is not as bad as the objective verification statistics suggest.

Table 5 shows the performance of the Nimrod analysis (and Model) in terms of Mean Factor Error (MFE) and Root Mean Square Factor Error (RMSFE). The analysis MFE of 1.00 and RMSFE of 2.24 suggest a reasonable fit to observations with no bias. Comparison with the Model is very favourable.

The subjective assessment is presented on a case-by-case basis for both analysis and forecast in section 7.4. However, the manual verification (described in section 7.4), suggests that, where fog is either present or diagnosed in a verification area, the analyses have a correct representation of its character and extent on 78 % of occasions.

7.3 Forecast Verification Results

The visibility forecast was assessed against the analysis for British Isles land points. The forecast was also compared with the Mesoscale Model prediction which would have been available operationally (T+5 to T+15 hours), and persistence (represented by the analysis at T+0). Before assessment, the analysis and

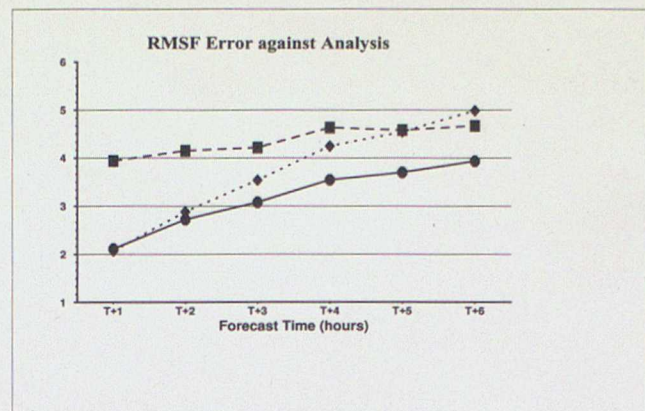


Figure 6: Forecast visibility Root Mean Square Factor Error against analysis: forecast=solid line, Model=dashed line, persistence=dotted line.

the field being verified were smoothed using a recursive Gaussian filter with a 25 km half-width at half-height, and thresholded at 1000 m and 200 m, conserving the original number of pixels with visibilities below the required threshold. From this, HR, FAR and CSI were calculated for both thresholds. The results are presented in graphical form for the 6 hours of the forecast in figure 5. At the 1000 m threshold, the forecast performance is quite good, with a high HR and a low FAR throughout the 6 hours, although the HR does drop rather rapidly in the first couple of hours of the forecast. The CSI scores show that the forecast is close to persistence at the start and close to the Model at the end, and overall better than both. At the 200 m threshold the results are poorer, with skill rapidly falling off. This may be partially owing to the assessment procedure, since the smoothing assumes that the main fog patches have a scale of at least 50 km, which may be inappropriate for thick fog. Comparison with persistence and the Model is favourable.

It is of interest to look at the performance of the forecast in terms of RMSFE (equation 38) against Analysis; unsmoothed fields are used for this comparison. Figure 6 shows the time series of RMSFE for the forecast, Model and persistence. The forecast is better than the other two throughout.

7.4 Individual Case Study Verification

Although it is instructive to look at the overall results from the 92 analyses and 14 forecasts, it is also useful to look at the performance for individual cases, which varies quite dramatically. Table 6 summarises the results of the objective area-based verification and the subjective verification for the analyses from the 6 cases with significant fog. The manual verification was carried out by considering areas which had either observed or analysed fog. For each area, the character and extent of the fog was assessed. As regards character, the differentiation between no fog (very small patches were ignored), patchy fog and extensive fog

Source	Areas Used	1000 m threshold				200 m threshold			
		Fog	HR	FAR	CSI	Fog	HR	FAR	CSI
Nimrod analysis	481	115	82%	20%	68%	35	23%	50%	19%
Mesoscale Model	481	115	63%	49%	39%	35	23%	43%	20%

Table 3: Analysis area-based HR, FAR and CSI for all cases using a 1000 m and 200 m threshold. 'Areas Used' indicates the number of areas verified, 'Fog' indicates the number of regions classed as foggy from observations.

Source	1000 m threshold				200 m threshold			
	Fog	HR	FAR	CSI	Fog	HR	FAR	CSI
Nimrod analysis	1176	83%	11%	75%	497	82%	12%	74%
Mesoscale Model	1176	45%	62%	26%	497	11%	74%	8%

Table 4: Analysis point-based HR, FAR and CSI for all cases using a 1000 m and 200 m threshold. 'Fog' indicates the number of foggy observations.

was made. The fog for an area was judged to be correct if the extent and character agreed with that suggested by surface observations; satellite imagery was used where possible to assist in this assessment. It can be seen that the scores range from 53 % for 9th November case to 95 % for 15th October, with an average of 78 %. The subjective scores are in broad agreement with the objective scores, but there are some differences. Figure 7 shows the CSI scores for forecast, Model and persistence for the 12 forecasts with significant fog. As with the analyses it can be seen that the quality varies significantly. To fully understand this it is necessary to look at the analyses and forecasts from some of the individual cases.

The 23rd December, 1994 was an interesting freezing fog case, which the Mesoscale Model handled very poorly. A ridge of high pressure extending from the continent over southern Britain resulted in slack winds across this area. This led to the development of fog which was very strongly tied to the orography with fog in the valleys, but clear over high ground. In a short article by Kidd (1994), very high resolution imagery from the French SPOT satellite shows this very well. Once the sun had risen, very marked temperature differences developed between the fog-bound valleys (as cold as -4°C) and the clear hill-tops (as warm as 5°C), on quite a small spatial scale. An 18 hour period from 00 UTC to 18 UTC was considered, giving a series of 19 analyses; three separate 6-hour forecast sequences generated from 00 UTC, 06 UTC and 12 UTC. At the start of the period areas of dense freezing fog were present over the South West and central southern England, and stretching along the Welsh border. During the study interval the distribution of fog changed slightly, with fog developing further east in central England and East Anglia. The case was covered by four separate runs of the Mesoscale Model, with data times at 18 UTC the previous day, and 00 UTC, 06 UTC and 12 UTC on

that day. The 18 UTC Model run had a reasonable representation of the fog distribution, but the other runs did not. They had fog in the East, rather than the West and completely cleared it during the day. At the start of the period (e.g. figure 8 shows the 04 UTC analysis), the analyses were, in general, good, primarily because of persistence being a good forecast (and dominating the 1 hour forecast). The exception was the eastern side of the country, where the analysis had too much fog; in reality, the fog only began to become widespread in East Anglia after about 06 UTC. The forecast from 00 UTC (figure 9) is dominated by persistence, which actually outperforms the forecast in the objective comparison (figure 7 top left). However, the forecast is good, and although it does not predict the fog in the West becoming more extensive, it does successfully predict the fog beginning to develop in East Anglia, providing better guidance than the Model. The 11 UTC and 12 UTC analyses are deficient in fog in the west, although better than the Model. However, with Meteosat imagery being used at both 12 and 13 UTC, the 13 UTC analysis (figure 10) is good, picking up the structure of the fog distribution well. By this time, the Model has almost completely lost the fog. After receding slightly in the middle of the day, the fog became more extensive again through the late afternoon. The analyses for the remainder of the period are fairly good although possibly not quite extensive enough. The Model is virtually devoid of fog, until it starts to reform at the end of the period. Although the Nimrod forecast from 12 UTC had insufficient fog, especially at T+1 and T+3, it was a great improvement on an almost clear Model prediction (figure 11).

The 24th July, 1995 case was chosen as a 'null case', having no significant fog. An anticyclone was positioned over the UK, with a weak front trailing across Scotland. Over southern England and the near continent it was clear and sunny, but cloud covered most

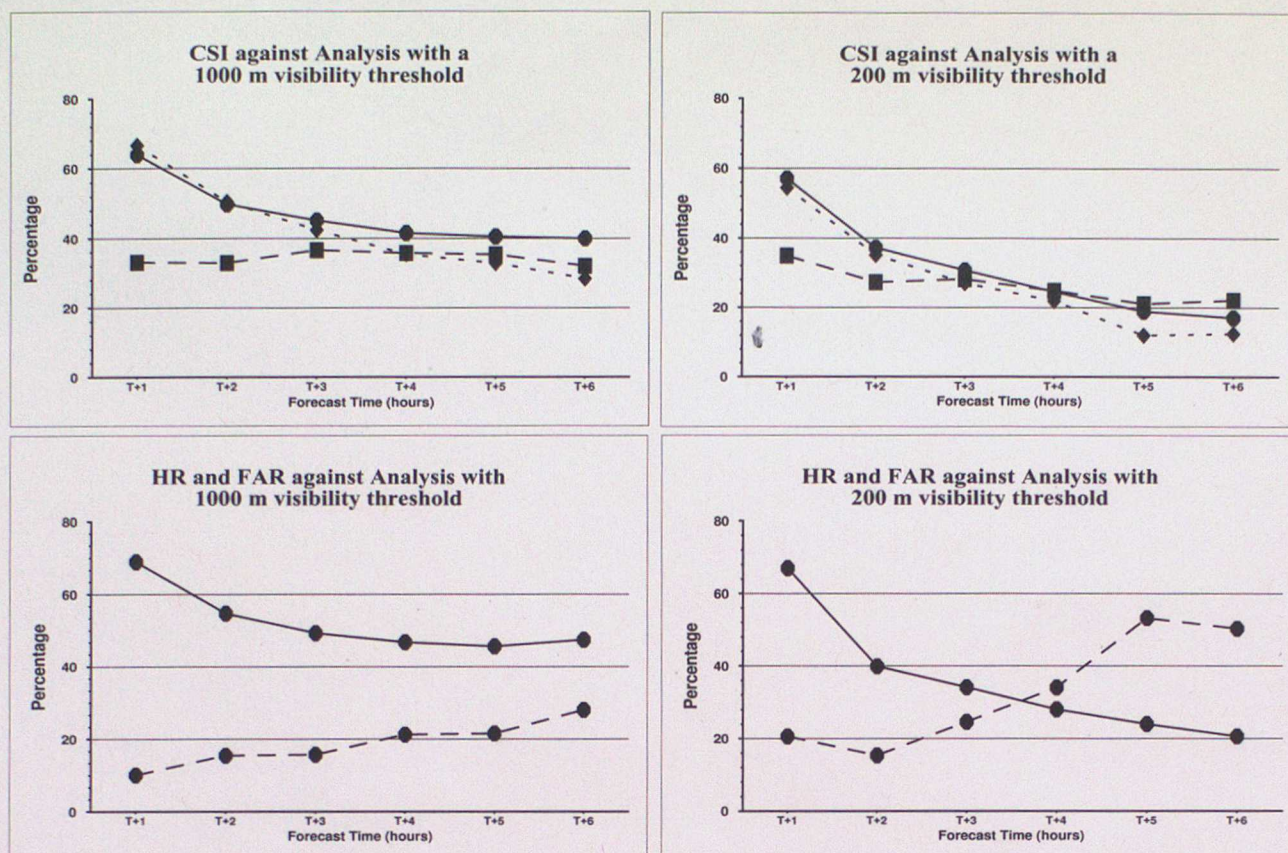


Figure 5: Visibility verification for all forecasts against forecast time: TOP: Critical Success Index (forecast=solid line, Model=dashed line, persistence=dotted line). BOTTOM: Forecast only: Hit Rate (solid line) and False Alarm Rate (dashed line), LEFT: With a 1000 m threshold, RIGHT: With a 200 m threshold,

Case date/times	1 km visibility			200m visibility			Extent & character	
	Obs	HR	FAR	Obs	HR	FAR	Obs	correct
00-18 UTC 23/12/94	37	84 %	9 %	20	5 %	0 %	147	86 %
18 UTC 13/10/95 -12 UTC 14/10/95	48	81 %	5 %	13	46 %	57 %	173	77 %
00-06 UTC 15/10/95	9	100 %	18 %	2	50 %	0 %	57	95 %
02-08 UTC 9/11/95	1	100 %	75 %	0	-	-	40	52 %
04-10 UTC 13/11/95	14	71 %	38 %	0	-	-	55	69 %
03-21 UTC 28/12/95	6	67 %	66 %	0	-	-	102	75 %
TOTAL	115	82 %	20 %	35	23 %	50 %	574	78 %

Table 6: A summary of the case study results for the visibility analyses. The Hit Rate and False Alarm Rate for each case and all cases are shown for thresholds of 1000 m and 200 m for verification areas 1, 2, 3, 4, 6, 9, 12 and 13. The number of observed 'foggy' regions is given in the column headed "Obs". The subjectively assessed percentage of regions/times for which the fog had the correct extent and character is also shown; the total number of regions considered is given in the column headed "Obs". Dashes indicate that the statistic can not be calculated.

of northern Britain. In general, visibilities were high, though some fog was observed in North Devon early in the morning. Two periods, spanning sunrise and sunset, were considered. The analyses and forecasts from both periods were, in general, good, keeping visibilities high.

On the night of the 13th October and into the morning of the 14th, widespread fog developed across southern and central England. Pressure was high on the

continent, with a weak southerly flow, to the south of a warm front, covering the UK. The whole of England was cloud-free throughout the period, apart from a patch of cloud which moved up across the country in the second half of the period. At the start, there was some fog on the coast of East Anglia and one report of fog on the South coast. During the night, the fog developed to cover most of southern and central England and East Anglia. The fog cleared through the follow-

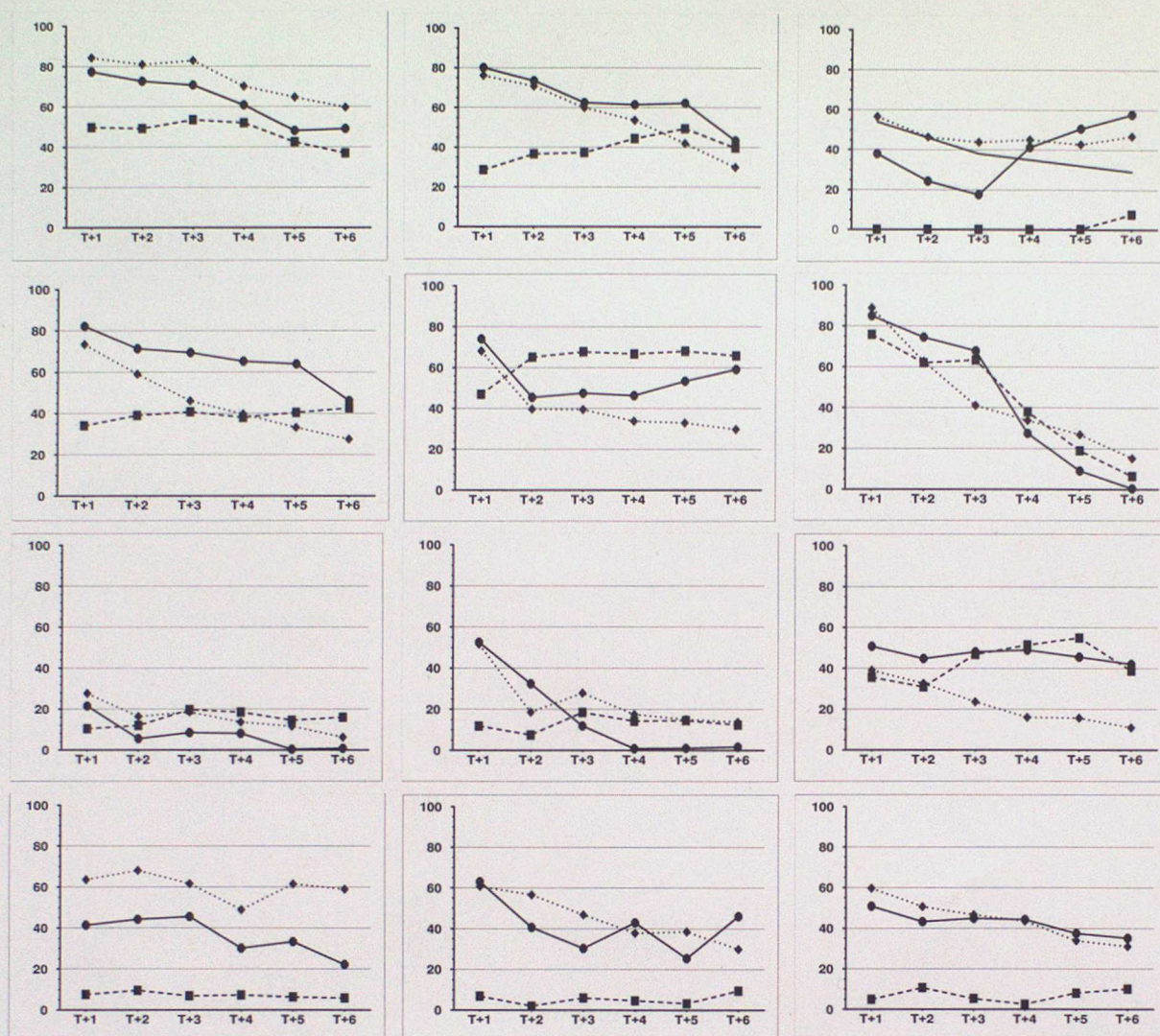


Figure 7: Critical Success Index against forecast time for comparisons of forecast against analysis for the individual cases (forecast=solid line, Model=dashed line, persistence=dotted line). Data times are: FIRST ROW: 00 UTC, 06 UTC and 12 UTC 23rd December, 1994, SECOND ROW: 18 UTC 13th October, 1995, 00 UTC and 06 UTC 14th October, 1995, THIRD ROW: 00 UTC 15th October, 1995, 02 UTC 9th November, 1995, 04 UTC 13th November, 1995, FOURTH ROW: 03 UTC, 09 UTC and 15 UTC 28th December, 1995.

ing morning to leave the country almost completely fog-free by midday. An 18 hour period from 18 UTC on 13th October to 12 UTC on the 14th was studied, giving a series of 19 analyses; three separate 6-hour forecast sequences were run from 18 UTC, 00 UTC and 06 UTC. In general the Model provided quite good guidance, except for an over-prediction of fog in Scotland and Ireland, which 'contaminated' the analyses (and forecasts) over these areas, where there are few observations to correct the first-guess. However, after sunrise, the Model cleared the fog and increased the visibilities far too quickly, possibly because of the absence of the observed patch of cloud over central England. The analysis represents the development of the fog over England fairly well, although the extent of the fog is probably too small. This assessment is complicated by the visibilities in these areas being around the 1 km threshold, with some stations going in and out of fog from hour to hour. The Model predicts the fog to be more extensive, especially from about 22 UTC on-

wards. The use of the AVHRR imagery at 02 UTC and 04 UTC produces substantially 'foggier', and almost certainly better, analyses (e.g. figure 12 shows the analysis for 04 UTC). Between 02 UTC and 07 UTC there are few major differences between the analysis and the Model, but the analysis has more structure, as would be expected; they are both good. At 08 UTC the fog began to clear. The Model clearance is too fast, and this has an indirect effect on the analysis, which has too little fog at this time. After 09 UTC the analyses are reasonable, possibly hanging on to too much fog in the Northwest of England. The forecast from 06 UTC is good out to about T+3, but its skill decreases rapidly after this (see figure 7 Panel 6), as does the skill of the Model and persistence, but this is primarily because of the near-complete clearance of the fog.

The 15th October case and the two November cases (9th and 13th) all have fronts over the country. The



Figure 9: Visibility (km) for 23rd December, 1994. LEFT: Model, MIDDLE: analysis, RIGHT: Nimrod forecast, FIRST ROW: 00 UTC (T+0 hour), SECOND ROW: 01 UTC (T+1 hour), THIRD ROW: 03 UTC (T+3 hours), FOURTH ROW: 06 UTC (T+6 hours).

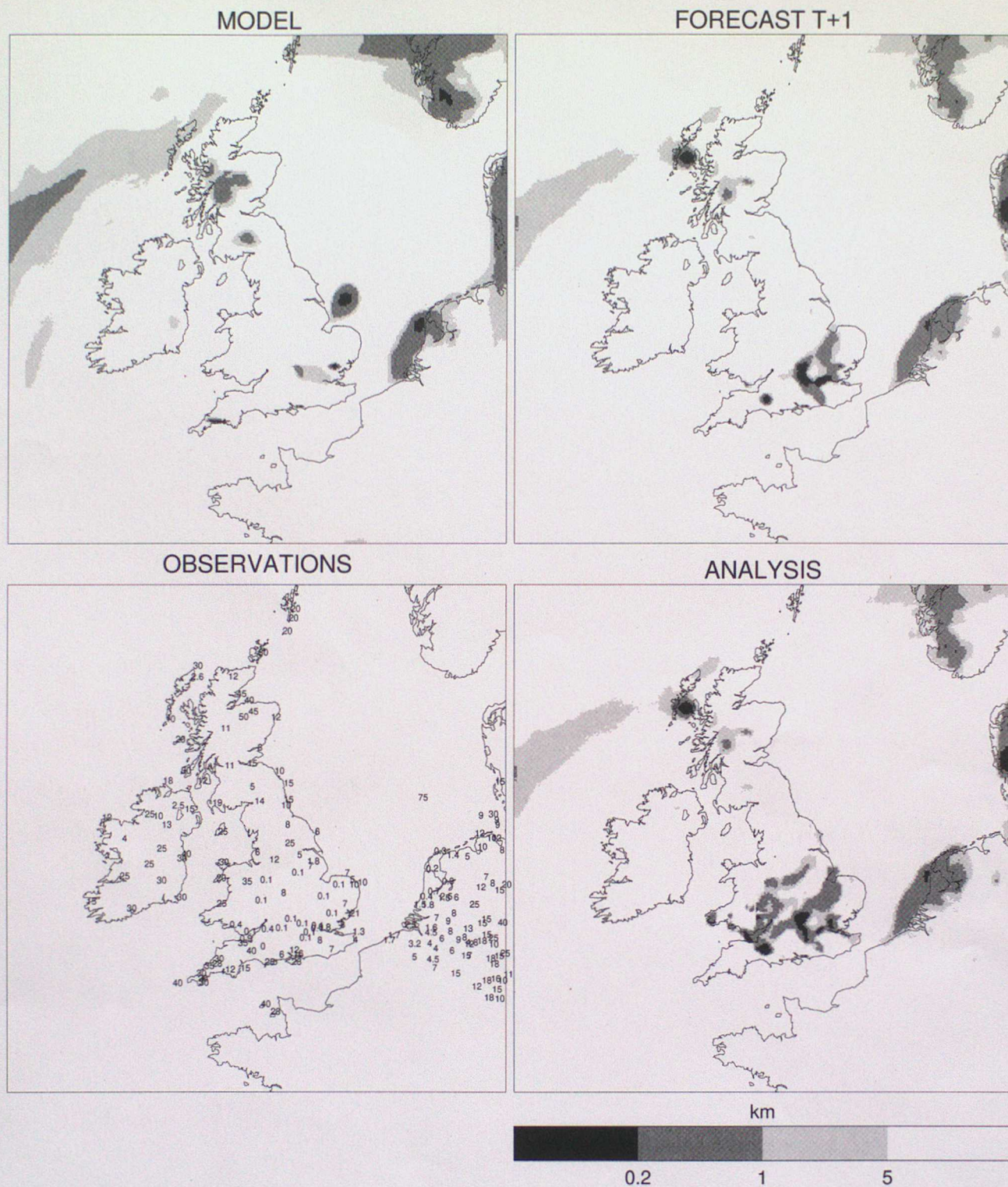


Figure 10: Visibility (km) for 13 UTC 23rd December, 1994. TOP LEFT: 7 hour Mesoscale Model forecast, TOP RIGHT: 1 hour Nimrod forecast, BOTTOM LEFT: visibility observations. BOTTOM RIGHT: analysis.

tive verification of the analyses quite difficult, but they appeared to be very good, although not having quite enough fog along the Northeast coast at the end of the period. However, the forecasts from 00 UTC are quite poor, as are the Model predictions (figure 13, and also figure 7 Panel 7). As well as over-predicting the fog, the Model has a poor representation of the distribution, putting much of the fog on the front rather than ahead of it. The forecast has very little fog, although

what it does have is approximately in the right place.

On the 9th November, a waving front was lying east-west across the centre of the country, with warm air to the south. The UK was completely covered by cloud throughout the period of interest, and although visibilities were poor, there was very little fog about. What fog was present was mainly confined to higher ground, although a more extensive area of fog did develop over Ireland towards the end of the period. A



Figure 11: Visibility (km) for 23rd December, 1994. LEFT: Model, MIDDLE: analysis, RIGHT: Nimrod forecast, FIRST ROW: 12 UTC (T+0 hour), SECOND ROW: 13 UTC (T+1 hour), THIRD ROW: 15 UTC (T+3 hours), FOURTH ROW: 18 UTC (T+6 hours).

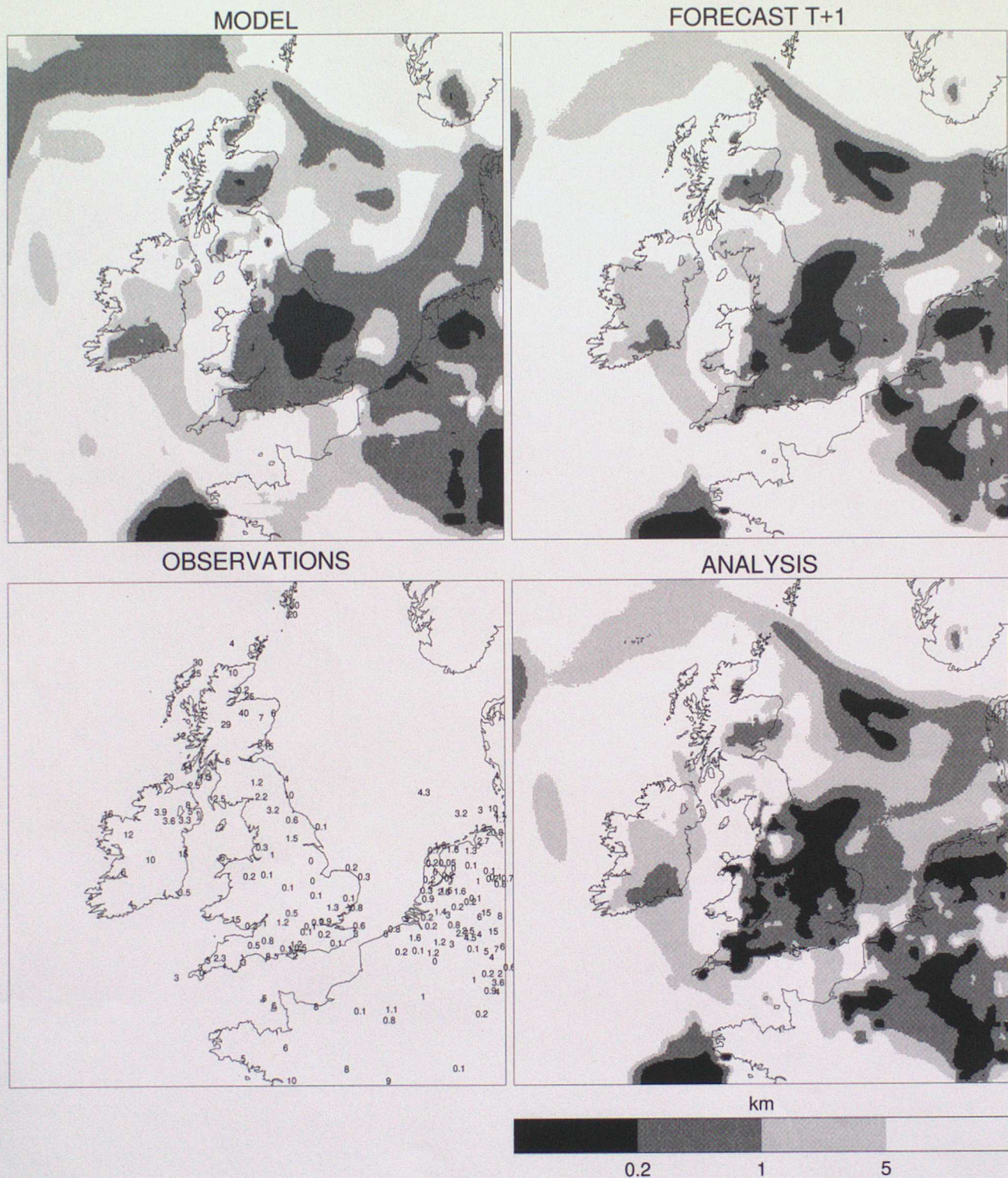


Figure 12: Visibility (km) for 04 UTC 14th October, 1995. TOP LEFT: 4 hour Mesoscale Model forecast, TOP RIGHT: 1 hour Nimrod forecast, BOTTOM LEFT: visibility observations. BOTTOM RIGHT: analysis.

6 hour interval spanning 02 UTC to 08 UTC was investigated, giving a series of 7 analyses; a forecast sequence was produced from 02 UTC. The analyses were poor throughout the period, but especially at the start, owing to 'contamination' by the considerable over-prediction of fog in the Model. Observations did correct this over central and southern England, but not in the data sparse regions of northern England and Scotland. Worse, over Ireland where visibili-

ties were not used (for reported visibilities over 10 km, the observed temperature and dew point are used to define T_L and q_t (see section 5.4)), fog was left in the analyses where visibilities were not even poor. For example, figure 14 shows the 06 UTC analysis. It can be seen that over central Ireland, a 3 km visibility observation, has produced a 'hole' in the spurious fog, whereas a neighbouring 16 km observation has not. This is a problem with not using the visibility in clear



Figure 13: Visibility (km) for 15th October, 1995. LEFT: Model, MIDDLE: analysis, RIGHT: Nimrod forecast, FIRST ROW: 00 UTC (T+0 hour), SECOND ROW: 01 UTC (T+1 hour), THIRD ROW: 03 UTC (T+3 hours), FOURTH ROW: 06 UTC (T+6 hours).

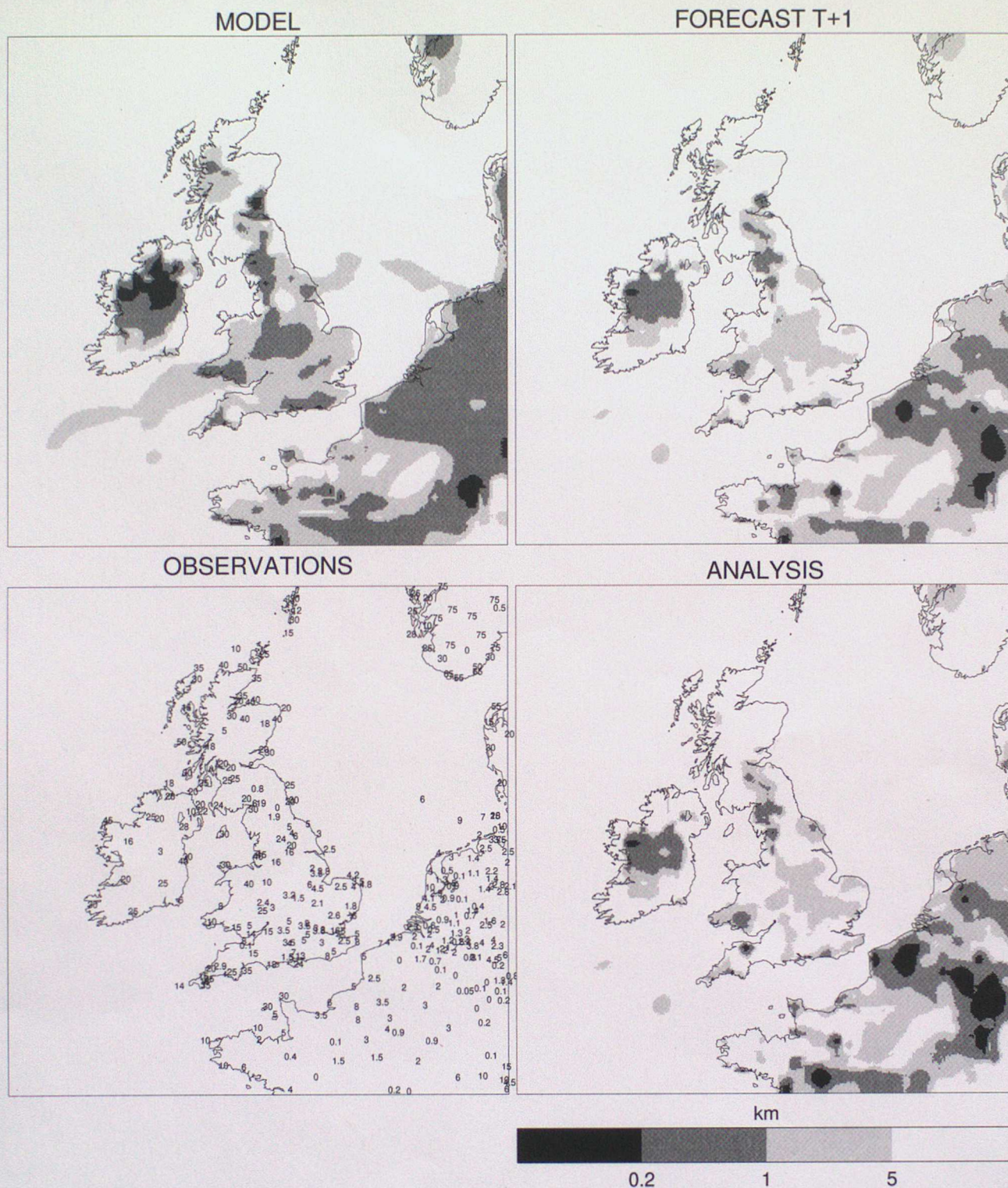


Figure 14: Visibility (km) for 06 UTC 9th November, 1995. TOP LEFT: 6 hour Mesoscale Model forecast, TOP RIGHT: 1 hour nimrod forecast, BOTTOM LEFT: visibility observations. BOTTOM RIGHT: analysis.

conditions, but is probably outweighed by the benefits in other situations. Fog does eventually form in Ireland through the period, and fog is observed over the high ground of northern England and the Southwest Peninsula. The forecasts are poor, as would be expected from a poor analysis.

The 28th December was another interesting freezing fog case. A ridge of high pressure extended westwards over Britain with a small closed centre over southern

Scotland. Winds were slack, and skies were cloud-free across all but the Southwest of England. This resulted in some very low temperatures over Scotland and areas of persistent freezing fog over central and eastern England. An 18 hour period from 03 UTC to 21 UTC was considered, giving a series of 19 analyses; three separate 6-hour forecast runs, from 03 UTC, 09 UTC and 15 UTC, were made. The Model has too little fog in England, and produces spurious fog around the coasts

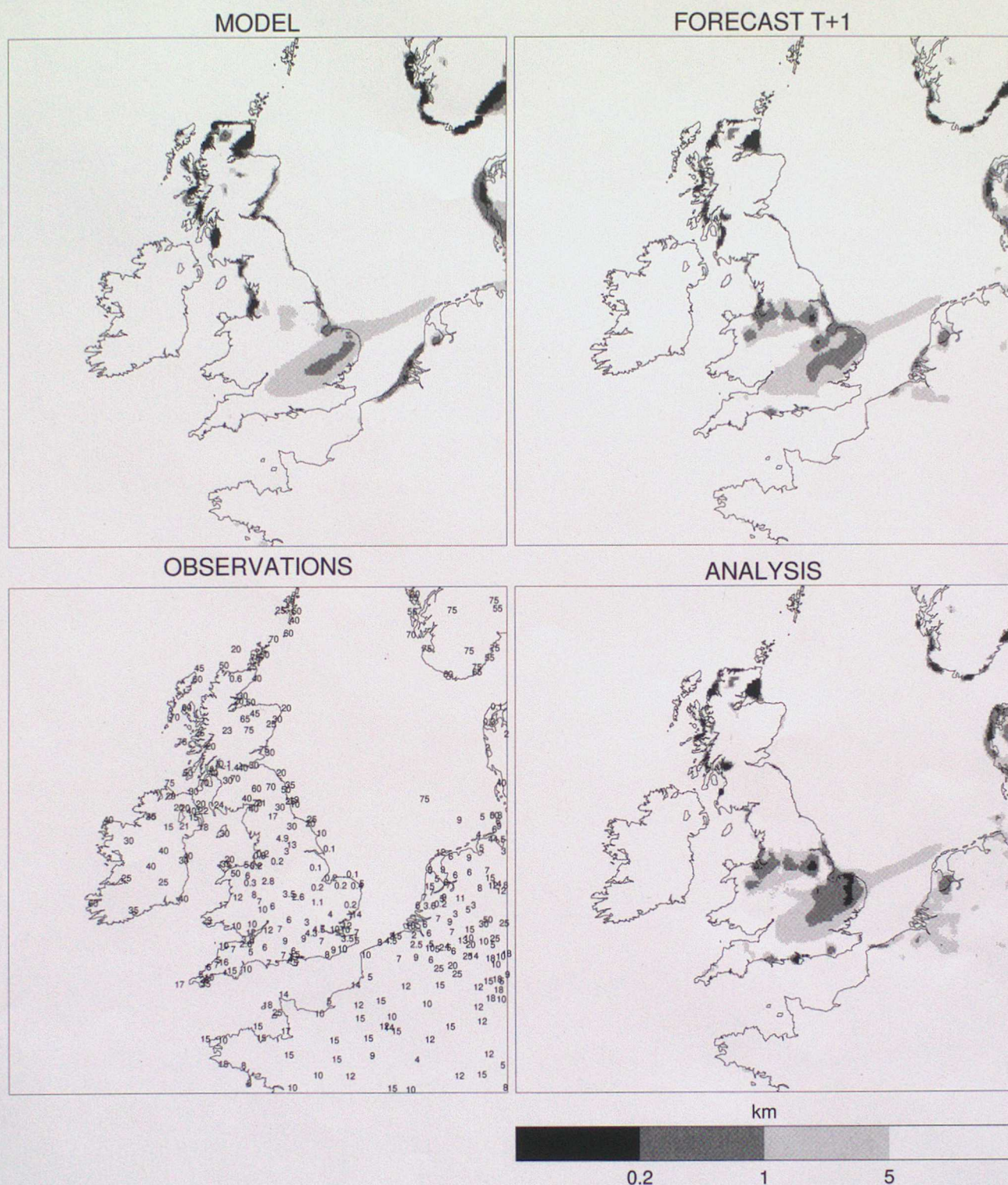


Figure 15: Visibility (km) for 09 UTC 28th December, 1995. TOP LEFT: 9 hour Mesoscale Model forecast, TOP RIGHT: 1 hour Forecast, BOTTOM LEFT: visibility observations. BOTTOM RIGHT: analysis.

of Scotland, which was probably the result of too much mixing between the very cold land air (typically -20°C) and the much warmer sea air. The analyses 'inherit' the problem of the Scottish coastal fog, as there are few observations to correct this, but this becomes less of a feature of the analyses throughout the period of interest. The fog in the South cleared very slowly from the south, which is represented reasonably well by the analysis (e.g. figure 15 shows the analysis for 09 UTC). The analysis probably has slightly too much fog, but

the problem is not as bad as implied by the statistics in table 6. As the changes happened very slowly, persistence was a good predictor, being objectively better than the forecast from 03 UTC and of similar quality to the Nimrod forecasts from 09 UTC and 15 UTC (see Figure 7 bottom 3 panels). Figure 16 shows the forecast from 09 UTC, which does not maintain enough fog, but is better than the Model guidance.

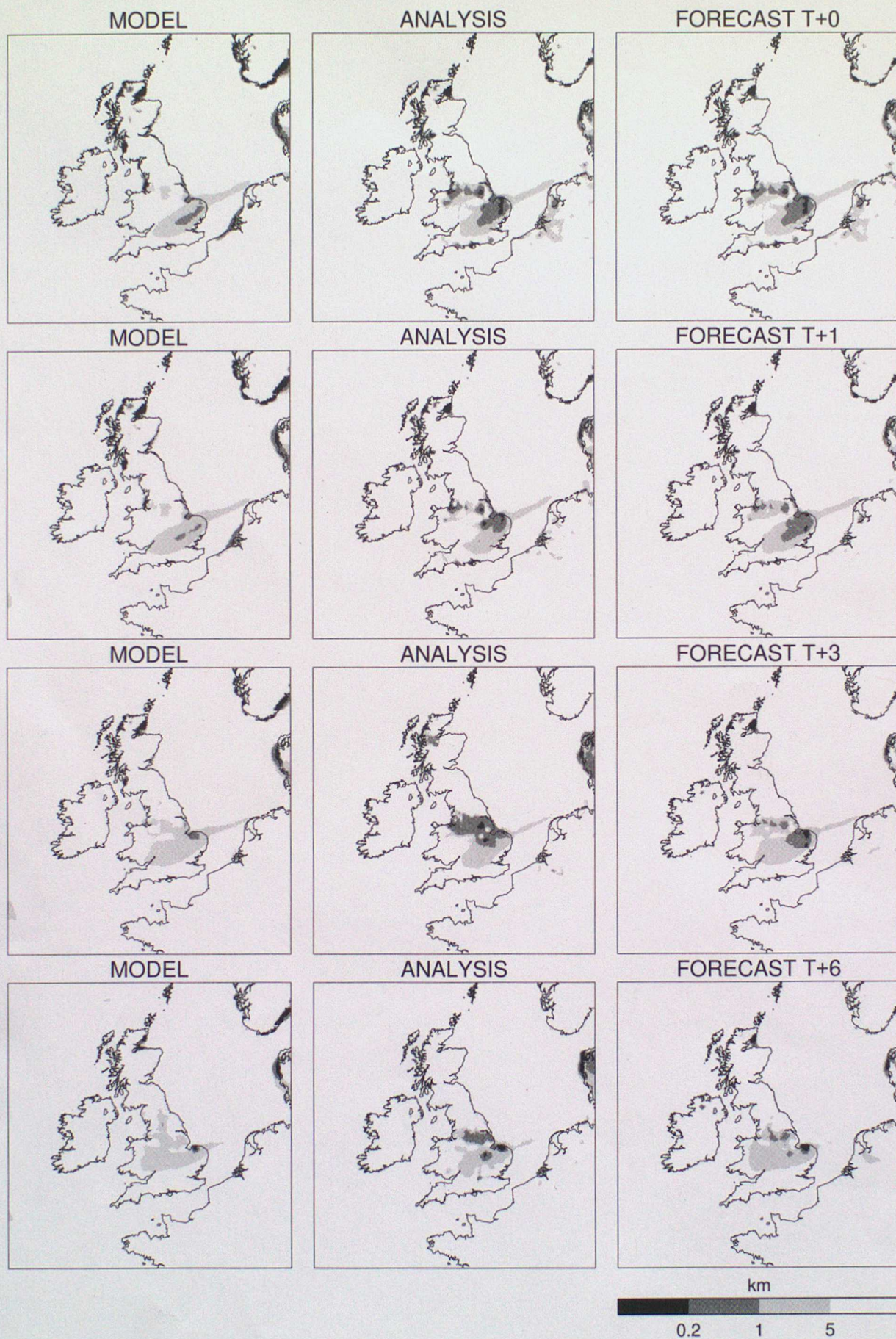


Figure 16: Visibility (km) for 28th December, 1995. LEFT: Model, MIDDLE: analysis, RIGHT: Nimrod forecast, FIRST ROW: 09 UTC (T+0 hour), SECOND ROW: 10 UTC (T+1 hour), THIRD ROW: 12 UTC (T+3 hours), FOURTH ROW: 15 UTC (T+6 hours).

8 Discussion and Summary

This paper has described in detail an objective Visibility Analysis/Forecast System (VAFS), which uses the prognostic variables liquid water temperature, T_L , and total water mixing ratio, q_t , from which visibility is diagnosed. Processed Meteosat and AVHRR imagery and surface observations are blended with a 1 hour forecast, using a variational algorithm, in which error correlations are represented through the application of a recursive filter. An extrapolation forecast is produced by adding trends in the prognostic variables, taken from the UKMO Mesoscale Model, to the analysis values. This is merged with the Model predictions and persistence, using time-varying, quality-dependent weights, to form the final forecast out to 6 hours.

The System has been tested on a number of case studies, from which both subjective and objective verifications have been presented. The analyses and forecasts generally produce a good representation of the visibility distribution. An area-based comparison with surface observations was the primary method of assessing the analyses; this approach assesses the fog extent and not just the fit to the data at observation points. Using a 1000 m visibility threshold, the results were good, with a Hit Rate (HR) of 82 % and a False Alarm Rate (FAR) of 20 % (a Critical Success Index (CSI) score of 68 %). However, with a 200 m threshold, they were poor: a HR of only 23 % and a FAR of 50 % (a CSI score of only 19 %), which implies little skill. This may, in part, be a problem with the area-based verification scheme which considers quite large areas. Thick fog tends to be patchy in nature, and so it is possible that the observations are not providing a good estimate of its areal extent. The forecasts were assessed against analyses. The time series of the Root Mean Square Factor Error shows the forecasts in a very favourable light, being close to persistence at the start of the forecast period and close to the Model at the end, but better than both throughout. A smoothed comparison of fog distribution was also made at both 1000 m and 200 m fog thresholds. The CSI score shows the forecast system to be similar or better than the Model and persistence at all times. The 200 m score decreases very rapidly, but this, once again, is probably because of the patchy nature of the fog, at least in part. The 1000 m fog threshold CSI score indicates reasonable skill throughout the forecast period.

The main weakness of the System tested here appear to be:

- a 'spin-up' from poor Model predictions
- a lack of satellite data
- poor handling of thick (200 m) fog

The first two of these weaknesses will be addressed by

a 'constant running' environment. The 'spin-up' problem will, of course, be absent. More Meteosat imagery should be available (owing to a change in processing), offering better high-resolution information on the fog distribution in the day, which will be carried forward in the analysis/forecast cycle. The poor performance in the handling of thick fog is probably because of a combinations of factors including the inherent difficulty in forecasting patchy fog and in verifying it sensibly. It may also be a consequence of the positioning of the observing sites; many are in low-land areas prone to fog, which might bias the observationally-assessed extent of the fog.

The VAFS will be run routinely for a winter trial (Winter 96-97) to allow further assessment. Acceptance of the system for operational use or the need for further improvements will depend on the results of this trial. The results of the trial are likely to be somewhat different from those of the case studies, owing to the greater variety of cases.

In summary, the VAFS presented here shows considerable promise, and offers significant improvements in skill over the corresponding Mesoscale Model predictions. The only further work planned before the winter trial is an adjustment in the use of the Model T_L and q_t values to allow for the difference in the Critical Relative Humidity values between the Model and the VAFS. This will ensure that the VAFS 'sees' the same Model visibilities as the Model, and will have the effect of a slight lowering of forecast visibilities. Although not discussed here, the use of the T_L and q_t variables allows the recovery of temperature and dew point in addition to visibility. These will be assessed separately with a view to their use in other very short range forecasting problems such as thunderstorm initiation and the onset of freezing.

9 Acknowledgements

Dr Brian Golding has supervised the development of the Visibility Analysis/Forecast System. Pete Clark, Dr Bruce Macpherson and Rod Brown have provided much useful advice. Steve Higginson carried out most of the data retrieval for the case studies.

References

- Ballard, S. P., Wright, B. J. & Golding, B. W. (1992), 'Diagnosis of visibility in the UK Met Office Mesoscale Model and the use of a visibility analysis to constrain the initial conditions'. *Met. Office Short Range Forecasting Research Div. Sci. Pap., No. 4*, pp 17+4pls. (Available from the National Meteorological Library, Bracknell, Berkshire, RG12 2SZ, UK.).

- Brown, R. & Roach, W. T. (1976), 'The physics of radiation fog: II — a numerical study', *Quart. J. R. Meteorol. Soc.* **102**, 335–354.
- Cullen, M. J. P. (1990), 'The unified forecast/climate model', *Meteorol. Mag.*, **122**, 81–94.
- Dybbroe, A. (1993), 'Automatic detection of the fog at night using AVHRR data', *Proc. 6th AVHRR Data Users' Meeting*, Belgirate, Italy, Eumetsat, **EUM P12**, 245–252.
- E04DGF—NAG Fortran Library Routine Document* (n.d.). *NAG Manual*, **3**, 14 pp.
- Ellrod, G. P. (1995), 'Advances in the detection and analysis of fog at night using GOES multispectral infrared imagery', *Weather and Forecasting* **10**, 606–619.
- Eyre, J. R., Brownscombe, J. L. & Allam, R. J. (1984), 'Detection of fog at night using Advanced Very High Resolution Radiometer (AVHRR) imagery', *Meteorol. Mag.* **113**, 265–271.
- Findlater, J., Roach, W. T. & McHugh, B. C. (1989), 'The Haar of north-east Scotland', *Quart. J. R. Meteorol. Soc.* **115**, 581–608.
- Fitzjarrald, D. R. & Lala, G. G. (1989), 'Hudson valley fog environments', *J. Appl. Meteorol.* **28**(12), 1303–1328.
- Golding, B. W. (1995), 'An integrated system for very short range forecasting', *Proc. Int. Conf. Meteorology and Hydrology Technology and Its Management*, Meteohytec 21, Geneva, **WMO/TD No. 672**, 114–117.
- Golding, B. W. (1996a), 'Nimrod: A system for generating automated very-short-range forecasts', *Submitted to Met. Apps.*
- Golding, B. W. (1996b), 'Short term forecasts of precipitation type', *Proc. 8th Int. Road Weather Conf.*, Birmingham, SIRWEC, 129–138.
- Kidd, C. (1994), 'Images of widespread radiation fog over southern England on 23rd December 1994', *Weather*, **50**, No. 11 (Nov.), 370–374, 377–378.
- Koschmeider, H. (1924), 'Theorie der horizontalen sichtweite', *Beitr. Phys. Atmosph.* **12**, 33–53, 171–181.
- Lorenc, A. C., Bell, R. S. & Macpherson, B. (1991), 'The Meteorological Office analysis correction data assimilation scheme', *Quart. J. Roy. Meteorol. Soc.* **117**, 59–89.
- Macpherson, B., Wright, B. J., Hand, W. & Maycock, A. J. (1996), 'The impact of MOPS moisture data in the UK Meteorological Office Mesoscale data assimilation scheme', *Mon. Wea. Rev.* **124**, 1746–1766.
- Pamment, J. A. (1994), 'Summary report on the tests of the automated cloud extrapolation forecast for Nimrod', *Met. Office FR Tech. Rep. No. 130*, pp 11+9pls. (Available from the National Meteorological Library, Bracknell, Berkshire, RG12 2SZ, UK.).
- Pruppacher, H. R. & Klett, J. D. (1978), *Microphysics of clouds and precipitation*, D. Reidel Publishing Company, Dordrecht, Holland.
- Roach, W. T., Brown, R., Caughey, S. J., Garland, J. A. & Readings, C. J. (1976), 'The physics of radiation fog: I — a field study', *Quart. J. R. Meteorol. Soc.* **102**, 355–359.
- Ryall, G. (1994), 'An automated system for generating very-short-range forecasts of precipitation', *D.Phil. thesis of University of Sussex*, pp xvii+301+119pls.
- Shurlock, J. S. & Lorenc, A. C. (1994), 'Two-dimensional grid-point variational analysis', *Met. Office FR-Div. Tech. Rep. No. 108*, pp 12+13pls. (Available from the National Meteorological Library, Bracknell, Berkshire, RG12 2SZ, UK.).
- Smith, R. N. B. (1990), 'A scheme for predicting layer clouds and their water content in a general circulation model', *Quart. J. Roy. Meteorol. Soc.* **116**, 435–460.
- Thomas, N. (1995), 'Fog and fog forecasts', *M.Sc. dissertation of University of Reading*, pp iii+96.